

Cellular Responses Associated with ROS Production and Cell Fate Decision in Early Stress Response to Iron Limitation in the Diatom *Thalassiosira pseudonana*

Chun-Shan Luo,[†] Jun-Rong Liang,^{*,†,‡} Qun Lin,^{§,†} Caixia Li,[†] Chris Bowler,^{||} Donald M. Anderson,[⊥] Peng Wang,[†] Xin-Wei Wang,[†] and Ya-Hui Gao^{†,‡}

[†]School of Life Sciences, Xiamen University, Xiamen 361102, People's Republic of China

[‡]Key Laboratory of the Ministry of Education for Coastal and Wetland Ecosystems, Xiamen University, Xiamen 361102, People's Republic of China

[§]School of Pharmaceutical Sciences, Xiamen University, Xiamen 361102, People's Republic of China

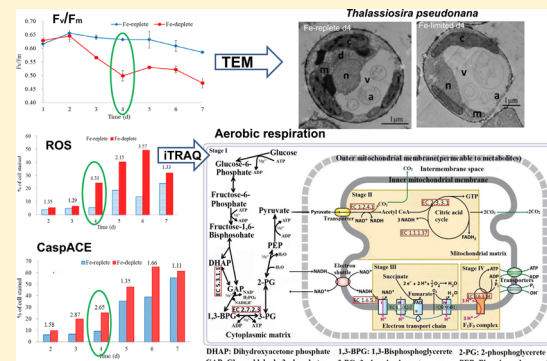
^{||}Environmental and Evolutionary Genomics Section, CNRS UMR8197 INSERM U1024, Institut de Biologie de l'Ecole Normale Supérieure (IBENS), Ecole Normale Supérieure, 46 rue d'Ulm, 75005, Paris, France

[⊥]Biology Department, Woods Hole Oceanographic Institution, Woods Hole, Massachusetts 02543, United States

Supporting Information

ABSTRACT: Investigation of how diatoms cope with the rapid fluctuations in iron bioavailability in marine environments may facilitate a better understanding of the mechanisms underlying their ecological success, in particular their ability to proliferate rapidly during favorable conditions. In this study, using *in vivo* biochemical markers and whole-cell iTRAQ-based proteomics analysis, we explored the cellular responses associated with reactive oxygen species (ROS) production and cell fate decision during the early response to Fe limitation in the centric diatom *Thalassiosira pseudonana*. Fe limitation caused a significant decrease in Photosystem (PS) II photosynthetic efficiency, damage to the photosynthetic electron transport chain in PS I, and blockage of the respiratory chain in complexes III and IV, which could all result in excess ROS accumulation. The increase in ROS likely triggered programmed cell death (PCD) in some of the Fe-limited cells through synthesis of a series of proteins involved in the delicate balance between pro-survival and pro-PCD factors. The results provide molecular-level insights into the major strategies that may be employed by *T. pseudonana* in response to Fe-limitation: the reduction of cell population density through PCD to reduce competition for available Fe, the reallocation of intracellular nitrogen and Fe to ensure survival, and an increase in expression of antioxidant and anti-PCD proteins to cope with stress.

KEYWORDS: diatom, iTRAQ-based proteomics, Fe-limitation stress, programmed cell death (PCD), reactive oxygen species (ROS), phytoplankton



INTRODUCTION

Diatoms are believed to be the most important primary producers in the ocean,¹ accounting for approximately 40% of total marine primary productivity.² These organisms are extensively distributed, are often dominant in well-mixed coastal and open-ocean upwelling regions,³ warm oligotrophic gyres,⁴ and the Southern and Arctic Oceans,⁵ and are even adapted to the subzero hypersaline conditions of brine channels within polar ice.⁶ Diatoms also grow rapidly with high turnover rates and often form massive blooms.^{1,7} It is of great interest to understand how and why diatoms have been able to achieve such remarkable prominence in contemporary oceans. It has been suggested that the ecological success of diatoms can be at least partially attributed to the unique mechanisms through which they cope with the wide range of fluctuations in the

complex marine environment, such as variations in the supply of nutrients (most notably nitrogen, phosphorus, silicon, and iron).

The critical roles of iron (Fe) in diatom growth and primary production are now well established. Phytoplankton growth in major high-nutrient, low-chlorophyll (HNLC) waters can be limited by Fe deficiency (e.g., Martin et al., 1991).⁸ Open ocean Fe-enrichment experiments in HNLC areas^{9–11} together with laboratory studies have demonstrated that diatoms have multilevel strategies to endure long-term (or chronic) Fe limitation (herein referred to as acclimated response). For low Fe quota diatom species such as *Phaeodactylum tricornutum*,

Received: May 14, 2014

Published: November 5, 2014



Thalassiosira oceanica, and *Pseudo-nitzschia multiseries*, several studies have indicated their unique high tolerance to chronic Fe-limitation stress and rapid responses to replenishment.^{12–16} However, *Thalassiosira pseudonana*, as a high Fe quota diatom species, has exhibited distinctive tolerance and different adaptation mechanisms in response to Fe-limitation conditions.^{13,17} For example the enhancement of photorespiration and pentose phosphate pathways have been proposed to be employed to acclimate to long-term Fe limitation (10 generations, almost 10 days), based on proteomics data.¹⁸ Another study has indicated that *T. pseudonana* cells display an early stress response at the onset of Fe limitation (the first 3 or 4 days) and then “acclimate” to Fe limitation on the following days, showing thus a physiological adjustment to Fe limitation from an early stress response to latter acclimated response.¹⁹ To date, although many studies have focused on the fundamental cellular response of diatoms to various Fe conditions such as Fe long-term stress, Fe-acclimation, Fe-spiking, and Fe-enrichment (see list of previous studies in Nunn et al., 2013¹⁸), studies of early stress responses in diatoms is very limited. Notwithstanding, it is likely that they often suffer from short-term Fe limitation (defined here as early stress response), particularly during bloom progression when they are likely to be subjected to rapid nutrient fluctuations, including rapid variations in Fe bioavailability.^{7,20} Therefore, it is necessary to investigate the cellular response and metabolic mechanisms through which diatoms respond to short-term iron limitation, which will help us elucidate how diatom cells control their life and death during blooms (termed cell-fate decisions). Despite the previous investigations of early morphological, and physiological responses²¹ as well as expression profiles of putative Fe-responsive genes (such as ferredoxin and flavodoxin)²² in early Fe-limited *T. pseudonana* cells, a molecular basis for early Fe-limited stress response has remained unclear. Actually, whole-cell proteomic profiling could be a powerful additional tool to describe the pathways and protein products involved in the early stress response to Fe-limitation, which could be distinct from acclimated responses.

Additionally, the response of *T. pseudonana* to Fe bioavailability suggests that Fe starvation and culture age can initiate programmed cell death (PCD).²¹ PCD is an irreversible, caspase-mediated, autocatalytic, and genetically controlled form of cell suicide that is accompanied by distinct morphological changes and an energy-dependent biochemical mechanism,²³ which is consistent with the markers of apoptosis in multicellular organisms.²¹ Over the past several decades, an increasing number of studies have noted that light limitation, nutrient starvation, and/or the accumulation of ROS can also induce a PCD process in unicellular phytoplankton,^{24–29} including in the diatom species *Ditylum brightwellii*,³⁰ *Thalassiosira weissflogii*,^{28,31} and *Skeletonema costatum*.³² Actually, a PCD response to Fe limitation is interesting given the importance of this trace metal in the regulation of diatom growth and primary productivity,²⁴ particularly during late-phase diatom blooms. In addition, it has been suggested that PCD resulting from Fe limitation is one of the main causes for the decline phase of phytoplankton (including of diatoms) blooms.^{33,34}

Related to PCD, the production of reactive oxygen species (ROS) has also been noted as a response to environmental stress.⁷ Despite the fact ROS exhibit several concentration-dependent functions,^{35,36} intermediate ROS concentrations are

considered to be toxic and to be able to trigger PCD.^{37,38} For instance, Vardi et al. (1999) reported that CO₂ limitation results in the formation of ROS to a level that induces PCD in the dinoflagellate *Peridinium gatunense*.²⁵ ROS accumulation induced by Fe limitation was also demonstrated to be involved in the triggering of PCD in *T. pseudonana*.¹⁹ Moreover, the colocalization of PtNOA (nitric oxide-associated protein) and Mn-superoxide dismutase (MnSOD) in the chloroplast of the diatom *P. tricornutum* is likely to be of relevance for ROS metabolism.^{26,39} Although the diatom responses to various adverse environmental factors may show some commonalities, ROS generation triggered by various stresses is generally attributed to different mechanisms.⁴⁰ Therefore, it is necessary to investigate the mechanisms of ROS production triggered by early stress of Fe limitation and their role in governing decisions related to cell-fate in diatoms.

As a complement to previous studies of cellular responses to Fe availability in *T. pseudonana*, a proteomics analysis was employed here to investigate its cellular responses associated with ROS production and cell-fate decisions during the early stress response phase of Fe limitation. Because PCD has also been found to be initiated in aging cultures,²¹ cells in the exponential phase of growth were chosen for the proteomics analysis. We combined *in vivo* biochemical markers with the well-developed iTRAQ-based (isobaric tags for relative and absolute quantitation) proteomics approach^{41,42} for the detection of the concomitant induction of ROS, caspase-specific activity, externalization of phosphatidylserine, cell death, and the suite of proteins involved in ROS production and cellular responses to oxidative stress. Our results address the biochemical machinery of ROS production triggered during the early stages of Fe limitation and the related cell-fate decision mechanisms, which is based on the balance of the functions of antioxidant and anti-PCD proteins and PCD-induced proteins. Furthermore, the data also provide a molecular-level understanding of the early stress response to Fe-limitation in *T. pseudonana*.

MATERIALS AND METHODS

Culture Conditions

Thalassiosira pseudonana (Hust.) Hasle et. Heimdal (strain CCMP 1335) was obtained from the Provasoli-Guillard National Center for Marine Algae and Microbiota (NCMA, formerly known as the CCMP, <https://ncma.bigelow.org/>). The culture was grown in f/2 medium at 18 °C under exposure to 60 micromol photons m⁻² s⁻¹ in a 12-h light/12-h dark regime. A starter culture of *T. pseudonana* was grown in f/2 medium to the midexponential phase (~3.0 × 10⁶ cells mL⁻¹). The cells were then pelleted via centrifugation (10 000×g, 18 °C, 10 min) and washed once with filtered (0.45 μm pore-size) autoclaved seawater (FSW) for inoculation of duplicate 4-L cultures of either replete f/2 medium (Fe-replete, +Fe) or f/2 medium without added iron (Fe-limited, -Fe) at a cell concentration of 1.5 × 10⁵ cells mL⁻¹. Seawater was collected from far offshore of Xiamen harbor and the seawater contained dissolved-Fe at very low concentrations. The duration of the experimental phase was 7 days.

Analysis of Physiological Parameters

Triplicate samples were collected daily and assessed for cell abundance and photosynthetic health. Cell numbers were counted using an Olympus microscope and a QiuJing hemocytometer at the same time every day.⁴³ The cell density

(cells mL^{-1}) was calculated as follows: $CD = (N/80) \times 400 \times 10^4$, where CD is the cell density, and N is the cell abundance counted in 80 grids on the slide.

The photochemical quantum yield of photosystem (PS) II (F_v/F_m) was measured by XE-PAM (Waltz, Germany). The measurements were performed in duplicate. Fifteen microliters of cells were harvested onto 2- μm -pore-size polycarbonate filters, snap frozen in liquid nitrogen, and stored at -80°C until F_v/F_m analysis. Ten milliliters of the filtered medium (0.45- μm pore size) was sampled daily and stored at -20°C for determination of nutrient concentrations.

Determination of Nitrogen, Phosphorus, and Silicon Concentrations

The concentrations of N— NO_3^- , P— PO_4^{3-} and Si— SiO_3^{2-} in the medium were measured daily according to classic colorimetric methods using a Technicon AA3 Auto-Analyzer (BRAN+LUEBBE, GmbH, Germany). N— NO_3^- was analyzed using the copper–cadmium column reduction method (Method No. G-172-96 Rev.7, BRAN+LUEBBE, Germany), P— PO_4^{3-} was determined by the molybdenum blue method (Method No. G-175-96 Rev.8, BRAN+LUEBBE, Germany), and Si— SiO_3^{2-} was measured using silicon–molybdenum blue spectrophotometry (Method No. G-177-96 Rev.5, BRAN+LUEBBE, Germany). The detection limits for N— NO_3^- , P— PO_4^{3-} and Si— SiO_3^{2-} were 0.015, 0.024, and 0.03 $\mu\text{mol L}^{-1}$, respectively.

Transmission Electron Microscopy (TEM)

The internal cell morphology of *T. pseudonana* cells was observed daily from day 2 by transmission electron microscopy (TEM). The cells were collected via centrifugation (4°C , 10 000 $\times g$, 5 min) and fixed in 500 μL of 2.5% glutaraldehyde fixative (pH 7.4) for 2 h. The cells were then rinsed once, resuspended in 0.1 M PBS (pH 7.4), and stored at 4°C (for less than 1 week) prior to the next treatment. The fixed cells were rinsed three times for 15 min in 0.1 M PBS (pH 7.4), postfixed for 2–3 h in 1% buffered OsO₄, and washed three times with 0.1 M PBS (pH 7.4). After the supernatant was removed by centrifugation (4°C , 10 000 $\times g$, 5 min), the pellets were dehydrated through a graded series of ethanol and then with propylene oxide. The cells were then embedded in an Epon812 Embedding medium (3 g of DDSA 3 g, 7 g of MNA, and 10 g of Epon812 in 0.32 mL of DMP). Sections were cut using a PowerTomo-XL ultramicrotome (RMC, U.S.A.), collected on 200-mesh copper grids, and stained with uranyl acetate and lead citrate. The stained sections were visualized and photographed using a H-7560 electron microscope (HITACHI, Japan).

In Vivo Cell Staining and Flow Cytometry

Cells were collected daily from day 2, pelleted via centrifugation (10 000 $\times g$, 10 min, 4°C), resuspended in buffer, and stained with the following: SYTOX green (1 μM ; Invitrogen) to visualize live/dead cells, z-VAD-FMK-FITC (20 μM ; CaspACE; Promega, Madison, WI, U.S.A.) to detect activated caspases, Annexin V (10 $\mu\text{L}/100 \mu\text{L}$ cells; Invitrogen) to detect the externalization of phosphatidylserine, and CM-H2DCFDA [5 μM ; 5-(and-6)-chloromethyl-2',7'-dichlorodihydrofluorescein diacetate, acetyl ester; Invitrogen] to detect intracellular ROS. The detailed protocol was previously described.¹⁹ The percentage of positively stained cells (from a total of 10 000 cells) was determined at 520 nm after excitation with a 488 nm laser using a flow cytometer (BD Fortessa, U.S.A.). The gating

and data analysis were performed using FlowJo analytical software.

Protein Extraction and Preparation

According to the physiological and biochemical results obtained for *T. pseudonana* during previous experiments, day 4 (middle exponential phase of growth) was chosen as the sampling time point for the iTRAQ-based proteomics analysis. Protein extraction was conducted according to the methods described by Du et al. (2014).⁴⁴ Briefly, approximately 1 L of culture was collected through a 2 μm pore-size filter membrane for each sample. Cells on the membrane were then resuspended with 10 mL medium into a 15 mL centrifugal tube. After the cell pellets were collected by centrifuging at 3000 $\times g$ for 5 min, 10 mL of TRIzol Reagent (Invitrogen, Life Technologies) was added, and the protein was then extracted according to the manufacturer's recommendations.

For protein preparation, the protein pellets were suspended in lysis buffer (7 M urea, 2 M thiourea, 4% CHAPS, 40 mM Tris-HCl, pH 8.5), then incubated with 10 mM DTT at 56°C for 1 h to reduce the disulfide bonds. After that, 55 mM IAM was added (final concentration), and the samples were incubated for 1 h in the dark to block the cysteine residues of the proteins (alkylate). The reduced and alkylated protein mixtures were precipitated by adding 4 \times volume of chilled acetone at -20°C overnight. After centrifugation on at 4°C , 30 000 $\times g$, the pellet was dissolved in 0.5 M TEAB (triethylammonium bicarbonate, Applied Biosystems, Milan, Italy) and sonicated in ice. After centrifuging at 30 000 $\times g$ at 4°C , an aliquot of the supernatant was taken for determination of protein concentration by Bradford Protein Assay Kit according to the manufacturer's protocol. The proteins in the supernatant were kept at -80°C until further analysis.

iTRAQ Labeling and SCX Fractionation

A total of 100 μg proteins from each sample were digested with Trypsin Gold (Promega, Madison, WI, U.S.A.) with the ratio of protein/trypsin = 30:1 at 37°C for 16 h. After trypsin digestion, peptides were dried by vacuum centrifugation. Peptides were reconstituted in 0.5 M TEAB and processed according to the manufacturer's protocol for 8-plex iTRAQ reagent (Applied Biosystems, Foster City, CA, U.S.A.). Four samples (two biological replicates for Fe-replete and Fe-limited, respectively) were labeled with different iTRAQ tags: 113- and 114-iTRAG tags for Fe-replete replicate 1 and 2, respectively; and 119- and 121-iTRAG tags for Fe-limited replicate 1 and 2, respectively. The peptides were labeled with the isobaric tags, and then incubated at room temperature for 2 h. The labeled peptide mixtures were then pooled and dried by vacuum centrifugation.

SCX (Strong Cationic Exchange) chromatography was performed using a Shimadzu LC-20AB HPLC pump system (Shimadzu, Kyoto, Japan). The fractionated peptides were first reconstituted in 4 mL of buffer A (25 mM NaH₂PO₄ in 25% ACN, pH 2.7) and then loaded onto a 4.6 \times 250 mm² Ultremex SCX column containing 5- μm particles (Phenomenex). The peptides were eluted at a flow rate of 1 mL/min with a gradient of buffer A for 10 min, 5–60% buffer B (25 mM NaH₂PO₄, 1 M KCl in 25% ACN, pH 2.7) for 27 min, 60–100% buffer B for 1 min. The system was then maintained at 100% buffer B for 1 min before equilibrating with buffer A for 10 min before the next injection. Elution was monitored by measuring the absorbance at 214 nm, and fractions were collected every minute. The eluted peptides were then pooled

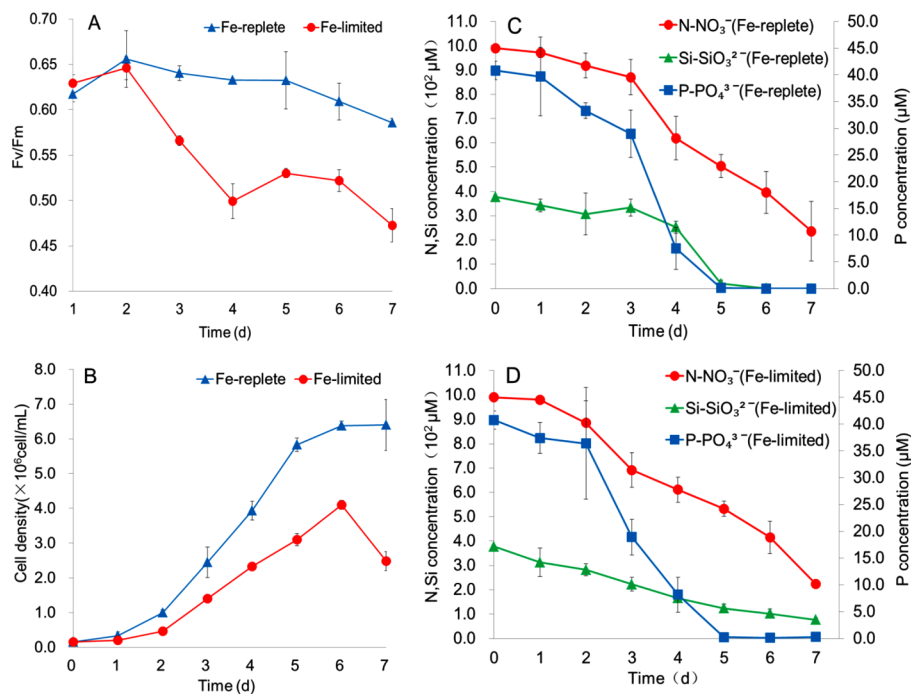


Figure 1. Growth, photosynthetic efficiency, and nutrient concentrations in Fe-replete and Fe-limited culture conditions. Photochemical quantum yield of photosystem II (F_v/F_m) (A) and cell growth (B) of *T. pseudonana* Fe-replete and Fe-limited cultures. The error bars represent the standard errors from duplicate measurements. Concentrations of N- NO_3^- , P- PO_4^{3-} , and Si- SiO_3^{2-} in media from *T. pseudonana* cells cultured under Fe-replete (C) and Fe-limited (D) conditions. The error bars represent the standard errors from triplicate measurements.

into 20 fractions, desalted with a Strata X C18 column (Phenomenex), and vacuum-dried.

LC-ESI-MS/MS Analysis

Each fraction was resuspended in solution A (2% ACN, 0.1% FA) and centrifuged at 20 000 $\times g$ for 10 min. The final concentration of peptide was about 0.5 $\mu g/\mu L$ on average. Ten μL supernatant was then loaded on a Shimadzu LC-20AD nano HPLC by the autosampler onto a C18 trap column, and the peptides were eluted onto an analytical C18 column (inner diameter of 75 μm) packed in-house. The samples were collected at a rate of 8 $\mu L/min$ for 4 min. A 44 min gradient was then run at a rate of 300 nL/min starting from 2% to 35% solution B (98% ACN and 0.1% FA), followed by a 2 min linear gradient to 80% solution B, maintenance at 80% solution B for 4 min, and return to 5% in 1 min.

The peptide samples were then subjected to nanoelectrospray ionization for tandem mass spectrometry (MS/MS) in a Q Exactive (Thermo Fisher Scientific, San Jose, CA, U.S.A.) coupled online to the HPLC. Intact peptides were detected in the Orbitrap at a resolution of 70 000. The peptides were chosen for MS/MS using the high-energy collision dissociation (HCD) operating mode with a normalized collision energy setting of 27.0 and a stepped NCE of 12.0%. The ion fragments were detected in the Orbitrap at a resolution of 17 500. A data-dependent procedure that alternated between one MS scan followed by 15 MS/MS scans was applied for the 15 most abundant precursor ions above a threshold ion count of 20 000 in the MS survey scan with subsequent dynamic exclusion duration of 15 s. The electrospray voltage applied was 1.6 kV. Automatic gain control (AGC) was used to optimize the spectra generated by the Orbitrap. The AGC target for full MS was 3e6 and 1e5 for MS2. For MS scans, the m/z scan

range was 350 to 2000 Da. For MS2 scans, the m/z scan range was 100–1800.

Proteomic Data Analysis

Raw data files acquired from the Orbitrap were converted into MGF files using Proteome Discoverer 1.2 (PD 1.2, Thermo), and the MGF file was searched. The peptide and protein identifications were performed through the Mascot search engine (ver. 2.3.02; Matrix Science, London, U.K.) against Joint Genome Institute database for the *T. pseudonana* genome (<http://genome.jgi-psf.org/Thaps3/Thaps3.home.html>, October, 2012, which contains a total of 34 736 sequences including the Thaps3 finished chromosomes and Thaps3_bd unmapped sequence data (386 sequences)) and NCBI.

For protein identification, a mass tolerance of 0.05 Da (the tolerance was “ ± 0.05 Da”) was permitted for intact peptide masses and ± 0.1 Da for fragmented ions, with allowance for one missed cleavage in the trypsin digests. Gln → pyro-Glu (N-term Q), Oxidation (M), Deamidated (NQ) as the potential variable modifications, and Carbamidomethyl (C), iTRAQ 8plex (N-term), iTRAQ 8plex (K) as fixed modifications. The charge states of peptides were set to +2 and +3. For reducing the probability of false peptide identification, only peptides at the 95% confidence interval by a Mascot probability analysis greater than “identity” were counted as identified.

For protein quantitation, it was required that a protein contains at least two unique peptides. The quantitative protein ratios were weighted and normalized by the median ratio in Mascot. The student’s *t* test was performed using the Mascot 2.3.02 software. We only used ratios with *p*-values <0.05, and only fold changes of >1.5 were considered as significant.

Function Annotation Description

Functional annotations of the proteins were conducted using Blast2GO program against the nonredundant protein database

(NR; NCBI). GO (Gene Ontology) enrichment analysis was carried out for the differentially regulated proteins to determine the affected cellular metabolism. Cluster of Orthologous Groups(COG, <http://www.geneontology.org>), a system for automated detection of homologues among the annotated genes of several completely sequenced eukaryotic genomes, was used to compare identified proteins to COG database for predicting the function of identical proteins and for functional classification and statistics.^{45,46} The analysis was performed by matching the responsive proteins to the proteins annotated with a COG term and then comparing the frequencies of the responsive proteins in each COG term subset to determine the statistical authenticity of the involvement of that COG term in the Fe-limited responses. A *P*-value of 0.05 was set as the threshold. KEGG pathway database (KEGG, <http://www.genome.jp/kegg/>), a collection of manually drawn pathway maps representing knowledge on molecular interaction and reaction networks, was used for protein functional and interaction analysis in different metabolic pathways.

Quantitative RT-PCR Analysis

The expression of 11 randomly selected genes encoding identified proteins was performed by quantitative RT-PCR analysis. The primers were designed using Primer-BLAST (Supporting Information, SI, Table S1).⁴⁷ Each primer pair was designed to span at least one exon–exon junction such that genome DNA digestion was not needed. At day 4, approximately 30 mL of culture was filtered for Fe-replete and Fe-limited conditions. Samples were rapidly placed in liquid nitrogen with the filter, ground to powder in a precooled traditional mortar, and immediately transferred to TRIzol Reagent (Invitrogen, Life Technologies). Total RNA was then extracted according to the manufacturer's recommendations. The cDNA was synthesized immediately after the RNA was extracted (ReverTra Ace qPCR RT Kit, TOYOBO, Japan). Quantitative PCR was performed with a Rotor-Gene 6000 system (Corbett Life Science) using the SYBR Green Real-time PCR Master Mix (TOYOBO, Japan). Each gene was detected in triplicate simultaneously with an inner control gene.

RESULTS AND DISCUSSION

General Physiological and Biochemical Responses

The cells were cultured under Fe-limited conditions ($f/2+Si$ medium without Fe added) and Fe-replete conditions ($f/2+Si$ medium). The photosynthetic efficiency of PSII (F_v/F_m), an indicator of Fe limitation in the laboratory,¹³ was used as a rapid measure of the physiological status of *T. pseudonana*. On day 4, which corresponds to the exponential phase (Figure 1A), the value of F_v/F_m of the cells exposed to Fe-limitation conditions was markedly reduced, being 20% lower (~0.50) compared to Fe-replete cells (~0.63). After day 4, the value of F_v/F_m slightly increased, indicating that the cells were exhibiting some physiological adjustment to Fe limitation on days 5 and 6. The growth rate and maximum cell abundances of the Fe-limited cells on day 4 were much lower than those of the Fe-replete cells: 17% lower growth rate (~0.50 in limited versus ~0.63 in replete) and 41% fewer cells (~ 2.33×10^6 in limited versus ~ 3.93×10^6 in replete), respectively (Figure 1B).

The notable differences in the degree of in vivo cell staining for ROS production (oxidative stress), externalization of phosphatidylserine (a morphological characteristic of the early stages of PCD), caspase activity (caspases are a specific class of intracellular cysteinyl aspartate-specific proteases that

initiate and execute PCD in metazoans⁴⁸), and cell mortality (visualization of live/dead cells) between cells exposed to Fe-replete and -limiting conditions during days 2–7 are shown in Figure 2 and Table 1. After 4 days of exposure, 24% of the Fe-limited cells stained positive for ROS compared with 6% of the Fe-replete cells (Figure 2A). This observation indicates that Fe-limitation caused a most marked increase in ROS (more than 4-fold) on day 4 compared with the Fe-replete cells, although the percent of positive stained cells for intracellular ROS was not

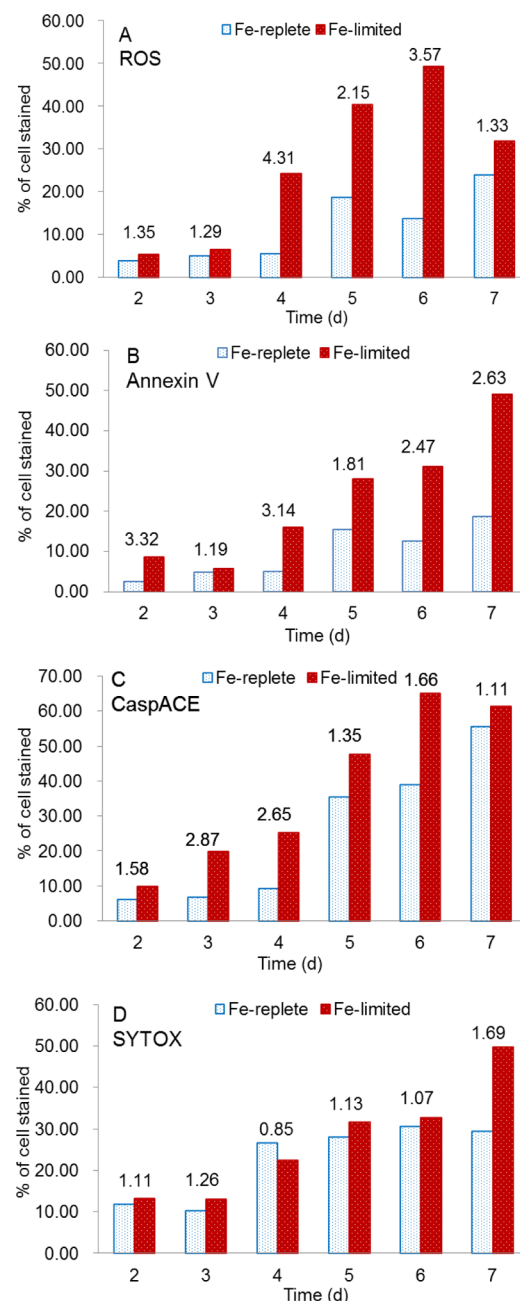


Figure 2. Examination of ROS production and PCD in cells grown in Fe-replete and Fe-limited conditions. In vivo detection of ROS (CM-H2DCFDA) (A), externalization of phosphatidylserine (Annexin V) (B), caspase activity (CaspACE) (C), and dead cells (SYTOX) (D) using flow cytometry. *T. pseudonana* cells were analyzed from days 2 to 7 after growth in either Fe-replete or Fe-limited media. The numbers above the columns represent the ratios of positive cells between Fe-limited and Fe-replete cultures.

Table 1. Percentage of Cells Positively-Stained for Intracellular ROS, Externalization of Phosphatidylserine, Caspase Activity, and Dead Cells Based on the in Vivo Staining of *T. pseudonana* Cells from Days 2 to 7 in Fe-replete (+Fe) or Fe-Limited (-Fe) Conditions

time (D)	culture	ROS (%)	annexin (%)	caspases (%)	SYTOX (%)
2	+Fe	4.1	2.6	6.5	11.9
	-Fe	5.5	8.6	10.2	13.2
3	+Fe	5.1	4.8	7.0	10.3
	-Fe	6.6	5.7	20.0	13.0
4	+Fe	5.7	5.1	9.6	26.6
	-Fe	24.4	16.0	25.4	22.5
5	+Fe	18.8	15.5	35.5	28.1
	-Fe	40.4	28.0	47.8	31.7
6	+Fe	13.8	12.6	39.2	30.7
	-Fe	49.3	31.1	65.2	32.7
7	+Fe	24.0	18.6	55.7	29.5
	-Fe	31.9	49.0	61.6	49.9

the highest on day 4. This result was consistent with the most marked decrease in F_v/F_m data on day 4 shown in Figure 1A, which indicates that the cells suffered from acute oxidative stress (early stress response) before attempting to physiologically adjust to the Fe-limited conditions after day 4. Correspondingly, the percent of positively stained cells for the externalization of phosphatidylserine (Annexin) (16%) and caspase activity (CaspACE) (25%) increased significantly by around 3-fold on day 4 in the Fe-limited cultures (Figure 2B,C). However, the ratio of dead cells was not significantly different between the Fe-limited and the Fe-replete cultures from days 2–6 (Figure 2D). These findings suggest that some cells were undergoing PCD due to intense oxidative stress on day 4 but were not actually dead.

To find further evidence that ROS induced PCD on day 4, we examined morphological changes based on TEM observations. The most common hallmarks of PCD previously recorded in *T. pseudonana*,²¹ such as marked vacuolization, internal degradation (unrecognizable organelles with integral membranes), and chromatin condensation, were indeed observed, as shown in Figure 3E. Morphological characteristics of PCD were also found in the cells on day 7 (Figure 3C,F) under both Fe-replete and Fe-limiting conditions, due to the fact that culture age also induces PCD.²¹ However, the nucleosomal laddering of DNA, the strongest evidence for PCD in higher eukaryotes, could not be detected (data not shown), which is consistent with the absence of ladders observed in previous studies of PCD in the same species,²¹ the dinoflagellate *Peridinium gatunense*,²⁵ and yeast.⁴⁹

General Results from the iTRAQ Analysis

To unravel the cellular responses associated with ROS production and cell-fate decision during the early stress response to Fe limitation, we harvested cells for iTRAQ-based proteomics analysis on day 4. We labeled and mixed two biological replicates of Fe-replete and Fe-limited samples directly for proteomic analysis. Reproducibility of the proteomics analysis for two comparison samples is shown in Figure S1 (SI), and Pearson correlation coefficients were used to evaluate the similarity between the two replicates. The delta error in the figure represents the difference between the quantitative values of two biological replicates of each treatment (Fe-replete or Fe-limited). The difference was plotted against the percentage of proteins identified, and the comparisons showed that approximately 50% of the proteins had differences with a delta error of less than 0.1, and more than 95% of the proteins had differences of less than 0.5 in both

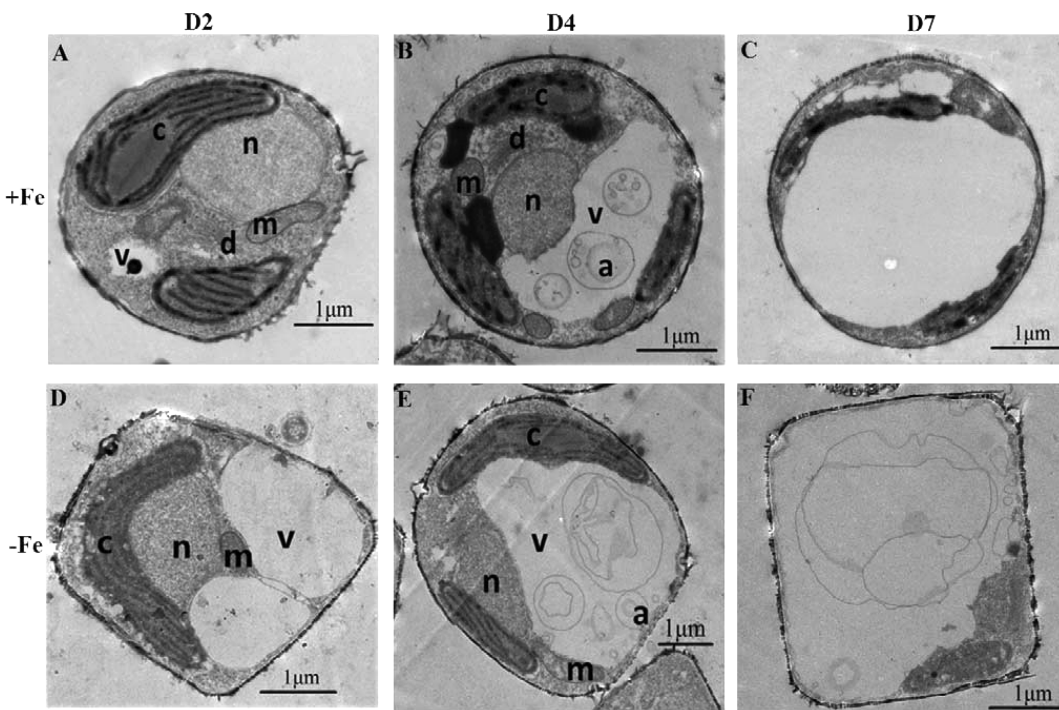


Figure 3. Electron micrographs of cells grown in Fe-replete and Fe-limited conditions. Morphological changes in *T. pseudonana* cells grown in Fe-replete conditions on day 2 (A), day 4 (B) and day 7 (C), and Fe-limited conditions on day 2 (D), day 4 (E), and day 7 (F). n: nucleus; c: chloroplast; m: mitochondria; d: dictyosome; v: vacuole; a: autophagosome; and bars: 1 μ m.

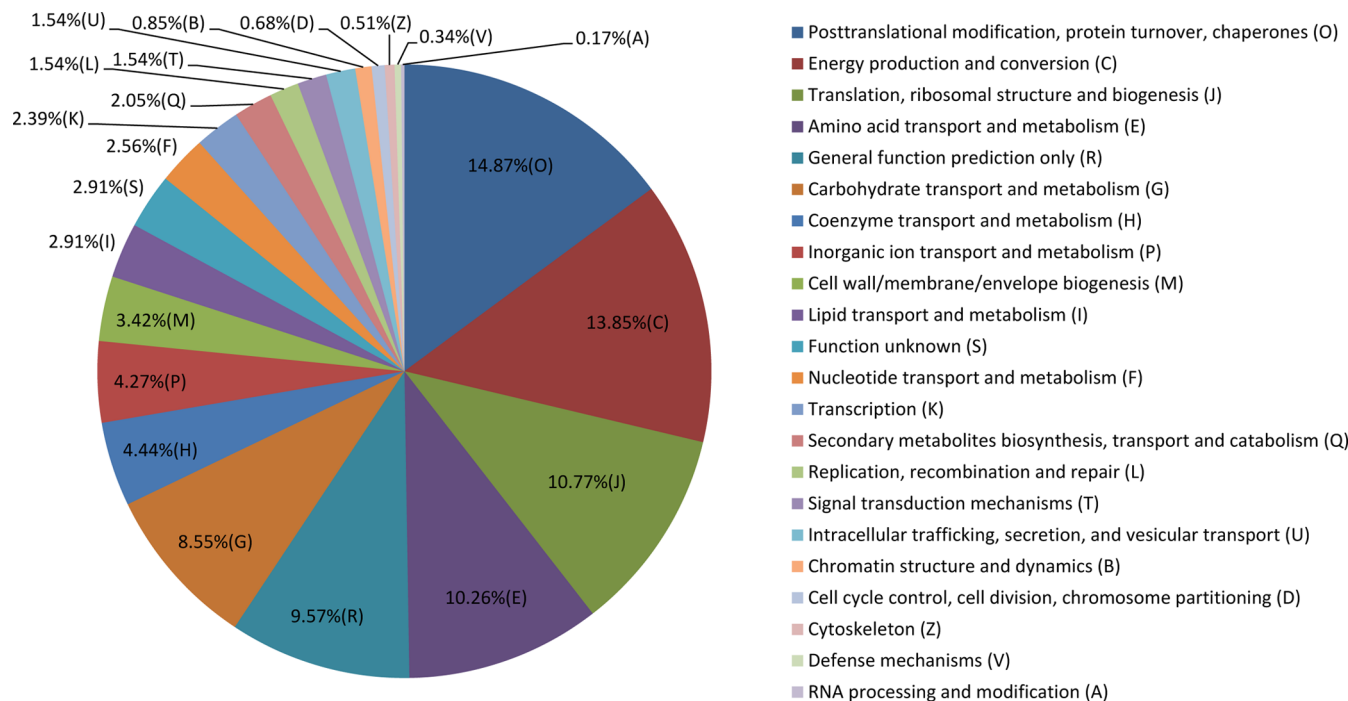


Figure 4. Functional category (COG) coverage of the proteins identified in *T. pseudonana* under Fe-limited conditions based on the iTRAQ-LC–MS/MS analysis.

treatments, suggesting good analytical reproducibility (SI Figure S1).

A total of 883 differentially regulated proteins between the Fe-replete and Fe-limited conditions were confidently identified in both biological replicates using the criteria described in the experimental methods (SI Table S2). Among these proteins, 510 were subjected to Cluster of Orthologous Groups (COG) enrichment analysis to determine the cellular metabolisms most impacted by Fe limitation (data shown in SI Table S3; 75 out of 510 proteins have more than one description). Functional classification of the proteins identified showed that they were involved in almost every aspect of *T. pseudonana* metabolism (Figure 4). Several key cellular processes, such as post-translational modification, protein turnover, and chaperones (14.9%), energy production and conversion (13.9%), translation, ribosomal structure and biogenesis (10.8%), and amino acid transport and metabolism (10.3%) were significantly affected by the Fe-limiting conditions. Furthermore, most of the “translation, ribosomal structure, and biogenesis” proteins identified were found to decrease in abundance, suggesting an overall slowdown of protein biosynthesis and a possible slowdown of metabolism.

Using a significance cutoff of 1.5-fold change and a *P*-value less than 0.05 to assess changes in abundance, we determined that a total of 127 proteins showed significant differences. Of these, 41 and 86 unique proteins, respectively, were found to be present in significantly higher and lower relative abundances in the Fe-limited cells compared with the cells exposed to Fe-replete conditions (SI Table S4). The most interesting proteins are summarized in SI Table S5.

Quantitative RT-PCR Analysis

A subset of 11 genes encoding the proteins detected in iTRAQ analysis was selected for quantitative RT-PCR analysis. The genes were selected based on the abundance levels of their encoded proteins to ensure that genes with a wide range of

- Posttranslational modification, protein turnover, chaperones (O)
- Energy production and conversion (C)
- Translation, ribosomal structure and biogenesis (J)
- Amino acid transport and metabolism (E)
- General function prediction only (R)
- Carbohydrate transport and metabolism (G)
- Coenzyme transport and metabolism (H)
- Inorganic ion transport and metabolism (P)
- Cell wall/membrane/envelope biogenesis (M)
- Lipid transport and metabolism (I)
- Function unknown (S)
- Nucleotide transport and metabolism (F)
- Transcription (K)
- Secondary metabolites biosynthesis, transport and catabolism (Q)
- Replication, recombination and repair (L)
- Signal transduction mechanisms (T)
- Intracellular trafficking, secretion, and vesicular transport (U)
- Chromatin structure and dynamics (B)
- Cell cycle control, cell division, chromosome partitioning (D)
- Cytoskeleton (Z)
- Defense mechanisms (V)
- RNA processing and modification (A)

expression levels were included, as well to cover a range of important regulatory processes. According to the iTRAQ proteomics analysis, the abundance of seven of the proteins encoded by the seven genes were decreased (i.e., Thaps3l 255232, Thaps3l2152, Thaps3l8571, Thaps3l25206, Thaps3l 24591, and Thaps3l1669), and four of the proteins encoded by the selected genes were increased in abundance (i.e., Thaps3l 20362, Thaps3l21534, Thaps3l3353, and Thaps3l2404). Eight of our quantitative RT-PCR results (Thaps3l255232, Thaps3l 2152, Thaps3l8571, Thaps3l25206, Thaps3l24591, Thaps3l 3353, Thaps3l2404, and Thaps3l1669) were somewhat consistent with the iTRAQ data, whereas three (Thaps3l 20362, Thaps3l21534, and Thaps3l11118) were not (Figure 5), indicating that their protein levels may not necessarily correlate with their mRNA levels. In particular, death-specific protein 1 (Thaps3l11118), an important protein associated with cell death and PCD regulation in phytoplankton (see below), was found at increased mRNA levels but decreased protein abundance. Another two proteins, a cyclin-dependent kinase (Thaps3l20362) and an RNA-binding protein (RRM domain) (Thaps3l21534), both showed decreased abundance of mRNA and increased abundance of protein.

Metabolic Mechanisms Involved in ROS Production

Downregulation of Photosynthesis and Accumulation of ROS. Light-harvesting complexes (LHCs) are generally used to harvest and transfer light energy into the reaction centers to drive photosynthesis.⁵⁰ Diatoms contain a branch of genes encoding the LHC superfamily known as fucoxanthin-chlorophyll a/c-binding proteins (FCPs).⁵¹ In the present study, Fe limitation induced the increased abundance of almost all of the FCPs, especially FCP 2 (Thaps3l30605, 1.60-fold, *p* > 0.05) and green algal LI818-like clade (annotated as LHCX in diatoms)^{51,52} (Thaps3l17894, 1.60-fold, Thaps3l12096, 1.48 fold). Recent studies have demonstrated that LHCX protein members have a dual role in light energy harvesting and excess

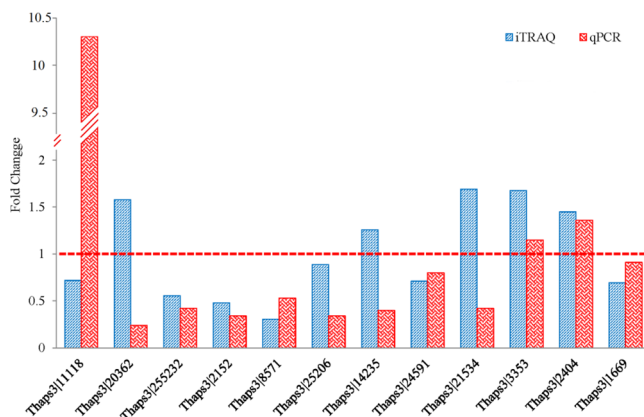


Figure 5. Comparison of iTRAQ and qPCR results for 11 genes. Comparison of the protein (iTRAQ) and mRNA (qPCR) levels of Thaps3|11118, Thaps3|20362, Thaps3|235232, Thaps3|2152, Thaps3|8571, Thaps3|25206, Thaps3|24591, Thaps3|21534, Thaps3|3353, Thaps3|2404, and Thaps3|1669 under Fe-limited conditions. β -actin was used as a housekeeping marker. Fold changes of either more than 1 or less than 1 from iTRAQ and qPCR indicate that they are consistent (red dotted line).

light energy dissipation.^{51,52} Moreover, the increased protein abundance and transcript level of FCP in Fe-limited *T. oceanica* cultures have been hypothesized by Lommer et al. (2012)¹² to be associated with light-mediated oxidative stress. One gene of the LHCX family was also found to be significantly up-regulated in Fe-limited *P. tricornutum* cells.¹³ Thus, the increased levels of these FCP proteins could infer that Fe-limited *T. pseudonana* cells were undergoing oxidative stress.

The abundance of proteins involved in PS II, such as photosystem II reaction center protein D2 (Thaps3|bd1272, 1.39 fold, $p > 0.05$), photosystem II oxygen-evolving complex 23K protein (Thaps3|2185, 1.22 fold, $p > 0.05$), and photosystem II 44-kDa reaction center protein (Thaps3_bdl1244, 1.23 fold), were increased slightly in our study (Figure 6), resulting potentially in a slight enhancement of PS II activity. The electrons produced in PS II must then be transferred to PS I by plastoquinone and the cytochrome *b6f* complex (cyt *b6f*), to ultimately lead to ATP production. However, in this study, most of PS I-related proteins and cytochrome *f*, a component of cyt *b6f* (Thaps3_bdl106, 0.64 fold, $p > 0.05$), were decreased in abundance in the Fe-limited *T. pseudonana* cells. In addition, the abundance of ferredoxin-NADP⁺ reductase (Thaps3|25892), which catalyzes the last electron transfer from PS I

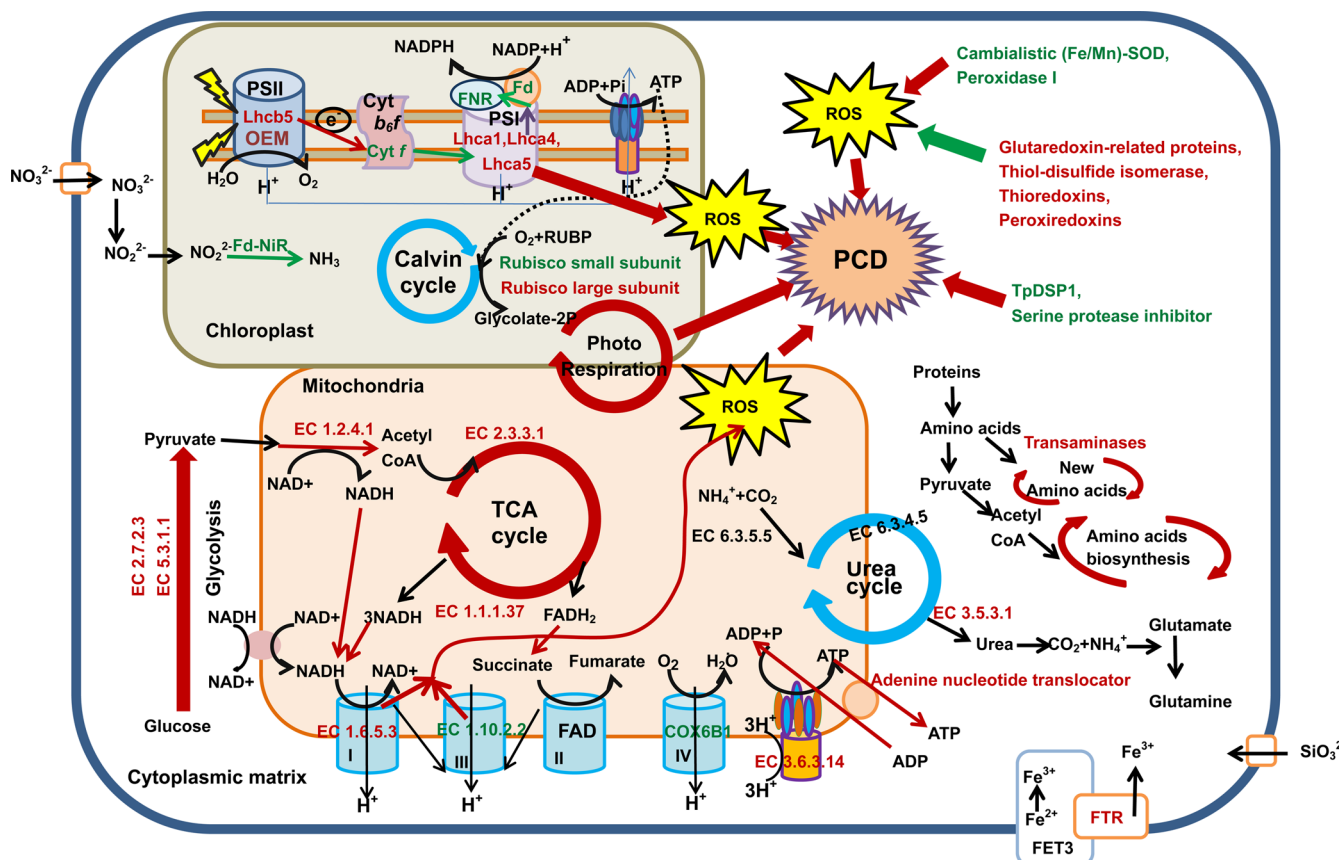


Figure 6. Hypothetical cellular pathways and processes in the diatom *T. pseudonana* under iron-limited growth conditions. All red words or arrows represent proteins with increased abundance or enhanced pathways, respectively. All green words or arrows represent proteins with decreased abundance or inhibited pathways, respectively. Lhc: Light harvesting complex; PS: Photosystem; OEM: Oxygen-evolving complex; Cyt: Cytochrome; FNR: Ferredoxin-NADP⁺ reductase; Fd: Ferredoxin; Fd-NiR: Ferredoxin nitrite reductase; ROS: Reactive oxygen species; PCD: Programmed cell death; RUBP: Ribulose-1,5-bisphosphate; TCA: Tricarboxylic acid cycle; FET3: Ferroxidase; FTR1: Iron permease; TpDSP: *T. pseudonana* death-specific protein; COX6B1: Cytochrome *c* oxidase subunit 6B1; EC 5.3.1.1: Triosephosphate isomerase; EC 2.7.2.3: 3-phosphoglycerate kinase; EC 1.2.4.1: Pyruvate dehydrogenase (E1) component; EC 2.3.3.1: Citrate synthase; EC 1.1.1.37: Malate/lactate dehydrogenases; EC 1.6.5.3: NADH-ubiquinone reductase; EC 1.10.2.2: Cytochrome *c1*; EC 3.6.3.14: ATP synthase; EC 6.3.5.5: Carbamoyl-phosphate synthase; EC 6.3.4.5: Argininosuccinate synthase; and EC 3.5.3.1: Arginase.

to NADP,⁵³ also decreased 0.56-fold. Therefore, the photosynthetic electron transport chain could be damaged in PS I, which could result in the accumulation of electrons and a concomitant increase in ROS generation. Furthermore, the abundance of some proteins associated with photosynthesis were also found to be slightly decreased, such as oxygen-evolving enhancer protein 1 precursor (Thaps3|16430, 0.29 fold, $p > 0.05$), high light-induced protein 2 (Thaps3|21467, 0.65 fold, $p > 0.05$), and ferredoxin (Thaps3_bdl1258, 0.55-fold), which further supports the existence of inefficient photosynthetic electron transport in Fe-limited *T. pseudonana* cells. In other words, Fe limitation caused the downregulation of photosynthesis and may block electron flow in PS I to result in the excess production of highly toxic ROS, which is consistent with previous results from the diatom *P. tricornutum*.¹³

Response of Cellular Respiration and ROS Accumulation. Under Fe-limited conditions, it was found that the three proteins involved in glycolysis, through which glucose is broken down into pyruvate with generation of a small amount of ATP and NADH, were markedly increased in abundance (Figure 6). These proteins are triosephosphate isomerase (EC 5.3.1.1, Thaps3|16639, 1.68-fold) which catalyzes the reversible interconversion of the triose phosphate isomers dihydroxyacetone phosphate and D-glyceraldehyde 3-phosphate, and 3-phosphoglycerate kinase (EC 2.7.2.3, Thaps3|14980, 1.55-fold and Thaps3|256275, 1.54-fold), an enzyme that catalyzes the reversible transfer of a phosphate group from 1,3-bisphosphoglycerate (1,3-BPG) to adenosine diphosphate (ADP) and then produces 3-phosphoglycerate (3-PG) and ATP. Thus, it could be inferred that more pyruvate would enter the mitochondrion and be fully oxidized to produce GTP, FADH₂, and NADH through the TCA cycle. At the same time, three proteins related to the TCA cycle were also significantly increased in protein abundance in the Fe-limited cells, including pyruvate dehydrogenase E1 (Thaps3|15834, 1.51-fold), citrate synthase (Thaps3|11411, 1.79-fold), and malate/lactate dehydrogenases (Thaps3|20726, 1.57-fold). The first protein (Thaps3|15834) is a component of the pyruvate dehydrogenase complex (PDC), which converts pyruvate into acetyl-CoA and links the glycolysis metabolic pathway to the TCA cycle. Citrate synthase catalyzes the first step of the TCA cycle, and the last protein, namely malate/lactate dehydrogenase, is an enzyme that reversibly catalyzes the oxidation of malate to oxaloacetate by the reduction of NAD⁺ to NADH. The increased abundance of these proteins could suggest that *T. pseudonana* may prefer to produce more NADH and FADH₂ and other bioenergy molecules by accelerating the decomposition of glucose in response to iron-limited stress.

The respiratory chain consists of a series of protein complexes that transfer electrons from NADH (or FADH₂) to O₂ via redox reactions. This chain includes coenzyme Q, cytochrome c, and four membrane-bound complexes (Complexes I, II, III, and IV) (Figure 6). In the present study, it was found that NADH-ubiquinone reductase (H⁺-translocating) (EC 1.6.5.3, Thaps3_bdl1380) in Complex I was markedly increased in abundance (1.7-fold), which may suggest that more electrons could be delivered to the respiratory chain in Fe-limited cells. However, both abundance of cytochrome c1 (Thaps3|25564, 0.56-fold) of Complex III and a possible cytochrome c oxidase subunit 6B1 (COX6B1, Uniprot_Swissprot, Thaps3|1996, 0.48-fold) of Complex IV were significantly decreased, which could indicate that Complexes III and IV were

inhibited and thus that the respiratory chain was blocked and electrons were undeliverable. In general, the major sites for ROS generation are Complexes I and III of the electron transport chain.^{54,55} Previous studies have also indicated that the oxidation of either Complex I or Complex II substrates when Complex III is inhibited by antimycin A may increase ROS accumulation.^{56,57} Thus, it can be proposed that under the Fe-limited conditions in the present study, increases in ROS production are likely to occur when Complex III is inhibited. Although cytochrome c oxidase is not a source of ROS,^{58,59} the inhibition of cytochrome c oxidase due to the decreased abundance of COX6B1 may facilitate ROS production from Complex I or III.^{60,61} Therefore, our findings also suggest that the observed decreased abundance of COX6B1 could also be considered to be related with the overproduction of ROS. It was found that mitochondrial alternative oxidase (AOX) is used as an alternative electron acceptor to remove excess electrons in Fe limited *P. tricornutum* cells because it uses less iron.¹³ However, we did not find AOX protein expression in this Fe limited *T. pseudonana* based on our proteomic data.

In addition, the decrease in ATP production via the respiratory chain coincided with the blockage of the respiratory chain when *T. pseudonana* suffered from Fe-limited stress. In contrast, the abundance of three proteins belonging to the F1 region of FoF1-type ATP synthase (an important enzyme that catalyzes the synthesis of ATP) were found to increase in response to Fe-limited stress in this study, indicating an increase in ATP production. These proteins are F0F1-type ATP synthase α subunit (Thaps3|13863, 1.52-fold), δ subunit (Thaps3|17981, 1.67-fold, $p > 0.05$), and ϵ subunit (Thaps3_bdl1254, 1.60-fold, $p > 0.05$), and all possess the core catalytic functions for the synthesis of ATP. Thus, it could be concluded that the increase in ATP synthesis observed in the present study may be a compensatory mechanism in response to the decrease in ATP production through the respiratory chain.

To conclude, evidence for the accumulation of ROS under Fe-limited conditions has been found to stem from inefficient activity of the electron transport chains in both the photosynthetic and respiratory processes (Figure 6). These results coincide with the high levels of intracellular ROS detected in vivo (Figure 2A), indicating that the cells were in a state of oxidative stresses.

Response to Oxidative Stress and Cell Fate Decision

Response to oxidative stress. Because oxidative stress can trigger PCD,^{37,38} *T. pseudonana* must have effective mechanisms for removing excess electrons and for scavenging ROS. On the other hand, due to Fe limitation, some typical ROS defense proteins that require iron as a cofactor showed limited abundance or even a decreased abundance. For example, superoxide dismutase (SOD, Thaps3|17168, 0.95-fold), which is a cambialistic (Fe/Mn)-SOD that has been previously cloned and characterized in the diatom *Thalassiosira weissflogii*,⁶² and catalase (peroxidase I) (Thaps3|257595, 0.68-fold), which is a tetramer of four polypeptide chains containing four porphyrin heme (iron) groups that allow the enzyme to react with hydrogen peroxide,⁶³ both showed decreased abundance. Notwithstanding, some other iron-free antioxidant enzymes were found to increase in abundance, presumably to replace these ROS scavenging functions. These included peroxiredoxins (Thaps3|32681, 1.64-fold), a ubiquitous family of antioxidant enzymes (peroxidases) to detoxify various

peroxide substrate,⁶⁴ which notably represent the second most highly abundant group of proteins found in this proteomics analysis. Moreover, glutaredoxin-related proteins (Thaps3l_261282, 1.26-fold) are thiol-disulfide oxidoreductases that can combat oxidative stress by detoxifying H₂O₂ to H₂O using glutathione and NADPH, and some members have been shown to exert anti-apoptotic effects.⁶⁵ The expression of thiol-disulfide isomerase and thioredoxins (Thaps3l_5491, 1.47-fold, Thaps3l_23961, 1.22-fold), the key antioxidant proteins in *T. pseudonana*,⁶⁶ were also elevated, which is consistent with the upregulation of the genes detected by Thamatrakorn et al. (2012).¹⁹ Our results indicate rather that an iron-free ROS scavenging machinery replaced the iron-rich systems to respond to the oxidative stress caused by Fe limitation.

In addition, some heat shock proteins showed differences in their expression levels under Fe-limited conditions. For example, chaperonin GroES (HSP10) (Thaps3l_24914, 0.29-fold), molecular chaperone GrpE (Thaps3l_18072, 0.64-fold), and some coexpression proteins, such as FKBP-type peptidyl-prolyl *cis-trans* isomerase 1 (Thaps3l_18543, 0.43-fold) and trypsin-like serine proteases (Thaps3l_875, 0.59-fold), all decreased in abundance. The decreased abundance of these proteins could reduce the tolerance of *T. pseudonana* cells to Fe limitation, inhibit growth, and other physiological processes, and eventually induce PCD. However, the increased abundance (1.56-fold) of chaperonin GroEL (HSP60 family, Thaps3l_13537) suggested that this anti-apoptotic protein is also present in the Fe-limited cells to resist the apoptotic process induced by Fe limitation. Furthermore, chaperonin GroEL, which is involved in protein folding after its post-translational translocation to the mitochondrion/chloroplast, has been suggested to play a key role in preventing the stress response⁶⁷ and apoptosis⁶⁸ in the cytoplasm.

Photorespiration is thought to play an important role in excess energy dissipation under stress conditions, such as high light or low temperature.⁶⁹ A similar function was also detected in Fe-limited cells of *P. tricornutum*.¹³ Ribulose-1,5-bisphosphate carboxylase/oxygenase (RuBisCO), the key enzyme used to fix CO₂ in photosynthesis,⁷⁰ also participates in photorespiration by consuming the O₂ created by photosynthesis (O₂ is a competitive inhibitor of CO₂).⁷¹ In the present study, the abundance of RuBisCO large subunit (Thaps3_bdl1265) (that has catalytic activity) increased (1.33-fold, *p* > 0.05), whereas the abundance of the RuBisCO small subunit (Thaps3_bdl1314) (that can functions as a CO₂ reservoir⁷²) decreased (0.87-fold, *p* > 0.05). This finding indicates that photorespiration may be strengthened to alleviate oxidative stress under Fe limitation.

PCD Induction. Internally triggered cell death has been identified in unicellular organisms⁷³ and may play a major role in phytoplankton bloom succession and collapse.^{24–26} ROS are one of the factors that can induce PCD. When oxidative stress exceeds the antioxidant capacity of cells, PCD pathways can be induced. In this study, based on the *in vivo* staining data and TEM observations, a markedly higher number of cells underwent PCD under Fe-limited conditions compared with Fe-replete conditions. Moreover, some proteins that are closely related to PCD processes were also detected in Fe-limited *T. pseudonana* cells.

As a case in point, the family of serine proteases comprises enzymes that cleave peptide bonds in proteins⁷⁴ and exhibit caspase-specific activity.⁷⁵ Our results showed that a serine protease inhibitor (Thaps3l_23814) decreased in abundance

(0.56-fold), which could suggest an increase in caspase-specific activity and the induction of PCD under Fe-limited conditions. In addition, the protein adenine nucleotide translocator has received much attention due to its participation in altering the integrity of the mitochondrial membrane, which promotes apoptosis.⁷⁶ The increased abundance (1.6-fold) of adenine nucleotide translocator (Thaps3l_260967) found in this study was in accordance with the typical features of PCD, as determined based on our morphological TEM observations (Figure 3E). Therefore, the protein data further confirmed that some cells were undergoing PCD in response to Fe limitation on day 4.

Furthermore, death-specific protein (DSP), which was first identified in the diatom *S. costatum*, has been suggested to play a role in the molecular mechanism of PCD in phytoplankton under stress.³² *T. pseudonana* has two DSP-like proteins (TpDSPs, namely TpDSP1 and TpDSP2), both of which have a transmembrane domain and calcium-binding EF-hand motifs.¹⁹ A recent investigation indicated that TpDSPs have a dual role in stress-acclimation and cell death based on the finding that the transcript levels of TpDSP1 and TpDSP2 genes are all markedly increased in response to sublethal and lethal ROS.¹⁹ Only one TpDSP, namely TpDSP1 (Thaps3l_11118), was detected in this study. Together with the *in vivo* staining results, which showed no difference in the ratio of dead cells between Fe-limited and Fe-replete cultures on day 4, the decreased abundance (0.72-fold, *p* > 0.05) of TpDSP1 implied that the TpDSP1 protein may play a role in cell death under Fe-limited conditions. According to the different expression patterns obtained for the TpDSP1 gene¹⁹ and protein (this study), which are also supported by our quantitative RT-PCR findings, we hypothesize that TpDSP may be subject to post-transcriptional regulation. However, more work is needed to confirm this hypothesis.

Unicellular organism PCD is considered an altruistic adaptation designed to benefit a population, as has been demonstrated in bacteria and yeast.^{77–80} Bidle et al. (2004) suggested that PCD may also have evolved in phytoplankton cells as a strategy to relieve a population from nutrient stress and remove aging and/or damaged cells from a population to ensure that they do not become a burden,²⁴ further supported by studies in *P. tricornutum* (Vardi et al. 2006). Therefore, in our study, PCD may be employed as a strategy to reduce the number of cells in the population, thereby decreasing the Fe demands of the whole population. Ultimately, the surviving cells would be able to grow better with an increased Fe supply under what would otherwise be Fe-limited conditions.

Other Cellular Responses to Fe Limitation

Intracellular Nitrogen Metabolism in Fe-Limited Cells. The use of nitrate can be restricted by Fe bioavailability because the enzymes involved in nitrate assimilation (nitrate reductase and nitrite reductase), require Fe as a cofactor. However, analysis of the nitrogen content in the medium showed that the assimilation of nitrate was not influenced by Fe limitation in our study, even showed an increase according to the consumption of per cell (Figure 1C,D). The proteomics data nonetheless showed that the abundance of ferredoxin subunits of nitrite reductase (Thaps3l_2673) were significantly decreased (0.60-fold), whereas the nitrate reductase of *T. pseudonana* was not detected (only one nitrate reductase [NADH] fragment (Thaps3l_24484) was detected and showed a slightly increased abundance (1.24-fold)). It can be inferred that *T. pseudonana*

cells exposed to early Fe limitation stress may continue to take up nitrate despite the decrease in reducing power (inactive nitrite reductase) and build up an internal pool of NO_2^- , which is in agreement with the findings reported by Milligan and Harrison (2000)⁸¹ and Allen et al. (2008).¹³ Furthermore, it is well-known that nitrite reductase requires five Fe atoms per active enzyme, whereas nitrate reductase only requires two. Thus, we speculate that nitrite reductase is affected prior to nitrate reductase upon exposure of *T. pseudonana* cells to early Fe limitation stress, whereas both enzymes may be affected during chronic Fe limitation.¹⁸ However, the genes for nitrate assimilation, such as nitrate reductase, two forms of nitrite reductase, and a plastid-targeted nitrite transporter, were all down regulated in Fe-limited *P. tricornutum* cells,¹³ suggesting differences in the responses of individual species to Fe limitation.

Moreover, some enzymes involved in intracellular amino acid metabolism, specifically cysteine synthase (Thaps3|14952, 1.82-fold, $p > 0.05$), methenyltetrahydrofolate cyclohydrolase (Thaps3|24746, 1.56-fold, $p > 0.05$), and glutamate dehydrogenase/leucine dehydrogenase (Thaps3|262098, 1.63-fold, $p > 0.05$), were found to increase in abundance in Fe-limited *T. pseudonana* cells. In addition, multiple aminotransferases, such as ornithine/acetylornithine aminotransferase (Thaps3|14668, 1.69-fold), aspartate/tyrosine/aromatic aminotransferase (Thaps3|14577, 1.63-fold), and serine-pyruvate aminotransferase/archaeal aspartate aminotransferase (Thaps3|22208, 1.58-fold), which are involved in amino acid reorganization and intracellular recycling, were also found to increase in abundance. The increased expression of the above-mentioned proteins could suggest that the intracellular recycling of N-containing compounds may be enhanced due to Fe-limitation stress. It is interesting that the aminotransferases detected in this study are totally different from the types of aminotransferases found in *T. pseudonana* cells when they underwent chronic Fe limitation stress.¹⁸ Thus, it can be hypothesized that different intracellular nitrogen-containing compounds may be reallocated due to different responses between the early and the acclimated stress response to Fe limitation.

Three enzymes associated with the ornithine-urea cycle (OUC) were also detected, specifically carbamoyl phosphate synthase large subunit (Thaps3|12265, 0.96-fold, $p > 0.05$), argininosuccinate synthase (Thaps3|25328, 1.27-fold), and arginase (Thaps3|16456, 1.78-fold, $p > 0.05$). However, other enzymes such as ornithine transcarbamoylase and arginino-succinase were not detected, and only arginase was found to be significantly increased in abundance in Fe-limited cultures compared with Fe-replete cultures. Arginase is an enzyme that catalyzes the final step in the urea cycle and converts L-arginine into L-ornithine and urea.^{82,83} In addition, the difference in the expression levels of the urease enzyme between the Fe-replete and Fe-limited cultures was not significant. Thus, the accumulation of urea may be as a nitrogen reserve to alleviate nitrogen deficiency caused by iron limitation in *T. pseudonana* based on the hypothesis that urea can also provide nitrogen to diatoms.⁸⁴ However, arginase was not detected and carbamoyl phosphate synthase was found to increase in abundance when *T. pseudonana* was acclimated to Fe limitation.¹⁸ These different responses of the OUC between the early stress response and the acclimated response indicate that different cellular strategies are employed.

Intracellular Iron Metabolism in Fe-Limited Cells. Fe acquisition by *T. pseudonana* occurs via a Fe(II) ferroxidase/

permease pathway, the molecular components of which consist of two ferric reductases (FRE1 and FRE2), two iron permeases (FTR1 and FTR2), a ferroxidase (FET3), and the divalent metal transporter NRAMP.^{15,19} However, only the plasma membrane iron permease (FTR1, Thaps3|20774) was detected and found to increase in abundance (1.54-fold) in this early stress response of Fe-limited cells, which is consistent with the acclimation response of *T. pseudonana* to Fe limitation¹⁸ (Nunn et al, 2013). This result suggests that a similar cellular strategy may be employed between these two responses, namely that *T. pseudonana* could increase production of FTR1 for Fe acquisition by endocytic recycling when limited by Fe.¹⁸

Moreover, the cells reduced their iron protein demands by using iron-free proteins with similar functions, e.g., ferredoxin was replaced by flavodoxin. In addition, proteins that do not require heme as a coenzyme or iron as a cofactor were found to increase in abundance during the antioxidant and anti-apoptotic processes reported here. Thus, we propose that the cell regulates its own protein expression to reduce the consumption of iron such that it is able to adapt to the environmental stress associated with iron limitation.

Intracellular Silicon Metabolism in Fe-Limited Cells

It is interesting that silicon uptake was also found to be enhanced by Fe-limitation (Figure 1). A higher silicon concentration in the medium was consumed under Fe-limited compared to Fe-replete conditions on day 4. Even the medium of Fe-replete cultures was completely depleted of silicon by day 5, while approximately 100 μm of silicon was still present in the medium of Fe-limited cultures. More silicon was taken up by Fe-limited cells than by Fe-replete cells on day 5, which was calculated based on the cell number. Our result is consistent with the previous finding that Fe limitation induced silica deposition in *T. pseudonana*, as demonstrated by the upregulation of the gene encoding silaffin 1 (a protein associated with silica deposition, SIL 1), as well as with the observation that the frustules of Fe-limited cells are thicker and more heavily silicified than Fe-replete cells (Mock et al, 2008).¹⁷ Our finding therefore support a possible link between iron bioavailability and silica deposition (Mock et al., 2008).¹⁷

CONCLUSIONS

In this study, iTRAQ proteomic profiles, in vivo biochemical markers and physiological characteristics represent not only a comprehensive systematic analysis of the early stress response of diatoms to Fe limitation, but also a large amount of information about previously uncharacterized cellular metabolism processes and proteins involved in ROS accumulation and PCD induction in response to short-term Fe limitation. Our observations provide a new molecular view about the diatom response to oxidative stress and control of cell fate: reduction of the cell population by PCD to reduce the consumption of Fe, enhancement of the turnover and reallocation of intracellular nitrogen and Fe into key cellular components to ensure the most basic survival and defense, and the increased abundance of antioxidant and anti-PCD proteins to ensure cell survival. These results significantly increase our understanding of how diatom cells control their life and death during blooms, and the molecular mechanism of diatoms involved in their survival and competition strategies to cope with trace metal fluctuations in the marine environment.

■ ASSOCIATED CONTENT

§ Supporting Information

Table S1. The primers designed for quantitative RT-PCR. Table S2. Full list of identified proteins of *T. pseudonana* and their ratio across conditions. Table S3. COG function classification of the differentially expressed proteins of *T. pseudonana* in Fe-limited conditions. Table S4. Proteins showing differential abundances in Fe-limited cells compared with those grown in Fe-replete conditions. Table S5. Abundances of some important proteins involved in a range of metabolisms under Fe-limited conditions. Figure S1. Reproducibility between biological replicates. Fe-replete biological replicates and Fe-limited biological replicates. This material is available free of charge via the Internet at <http://pubs.acs.org>.

■ AUTHOR INFORMATION

Corresponding Author

*Tel: 86 592 2184368; fax: 86 592 2181386; e-mail: sunljr@xmu.edu.cn.

Notes

The authors declare no competing financial interest.

■ ACKNOWLEDGMENTS

This work was supported by the National Natural Science Foundation of China (Grant No. 41076080 and 41276130) and the Fujian Province Science Fund for Distinguished University Young Scholars (Grant No. JA10001). C.B. acknowledges support from the ERC Advanced Grant Diatomite. Support for D.M.A. was provided through the Woods Hole Center for Oceans and Human Health, National Science Foundation Grant OCE-1314642 and National Institute of Environmental Health Sciences Grant 1-P01-ES021923-01. We also express our sincere thanks to the anonymous reviewers.

■ REFERENCES

- (1) Armbrust, E. V. The life of diatoms in the world's oceans. *Nature* **2009**, *459* (7244), 185–192.
- (2) Ragueneau, O.; Schultes, S.; Bidle, K.; Claquin, P.; Moriceau, B., Si and C interactions in the world ocean: Importance of ecological processes and implications for the role of diatoms in the biological pump. *Global Biogeochem. Cycles* **2006**, *20*, (4).
- (3) Brzezinski, M. A.; Jones, J. L.; Bidle, K. D.; Azam, F. The balance between silica production and silica dissolution in the sea: Insights from Monterey Bay, California, applied to the global data set. *Limnol. Oceanogr.* **2003**, *48* (5), 1846–1854.
- (4) Brzezinski, M. A.; Nelson, D. M. The annual silica cycle in the Sargasso Sea near Bermuda. *Deep Sea Res.* **1995**, *42* (7), 1215–1237.
- (5) Nelson, D. M.; Gordon, L. I. Production and pelagic dissolution of biogenic silica in the Southern Ocean. *Geochim. Cosmochim. Acta* **1982**, *46* (4), 491–501.
- (6) Bowler, C.; Vardi, A.; Allen, A. E. Oceanographic and biogeochemical insights from diatom genomes. *Ann. Rev. Mar. Sci.* **2010**, *2*, 333–365.
- (7) Rosenwasser, S.; van Creveld, S. G.; Schatz, D.; Malitsky, S.; Tzfadia, O.; Aharoni, A.; Levin, Y.; Gabashvili, A.; Feldmesser, E.; Vardi, A. Mapping the diatom redox-sensitive proteome provides insight into response to nitrogen stress in the marine environment. *Proc. Natl. Acad. Sci. USA* **2014**, *111* (7), 2740–2745.
- (8) Martin, J. H.; Gordon, R. M.; Fitzwater, S. E. The case for iron. *Limnol. Oceanogr.* **1991**, *36* (8), 1793–1802.
- (9) De Baar, H. J.; Boyd, P. W.; Coale, K. H.; Landry, M. R.; Tsuda, A.; Assmy, P.; Bakker, D. C.; Bozec, Y.; Barber, R. T.; Brzezinski, M. A., Synthesis of iron fertilization experiments: from the iron age in the age of enlightenment. *J. Geophys. Res.* **2005**, *110*, (C09S16).
- (10) Boyd, P. W.; Jickells, T.; Law, C. S.; Blain, S.; Boyle, E. A.; Buesseler, K. O.; Coale, K. H.; Cullen, J. J.; de Baar, H. J.; Follows, M.; Harvey, M.; Lancelot, C.; Levasseur, M.; Owens, N. P.; Pollard, R.; Ryklin, R. B.; Sarmiento, J.; Schoemann, V.; Smetacek, V.; Takeda, S.; Tsuda, A.; Turner, S.; Watson, A. J. Mesoscale iron enrichment experiments 1993–2005: synthesis and future directions. *Science* **2007**, *315* (5812), 612–617.
- (11) Behrenfeld, M. J.; O'Malley, R. T.; Siegel, D. A.; McClain, C. R.; Sarmiento, J. L.; Feldman, G. C.; Milligan, A. J.; Falkowski, P. G.; Letelier, R. M.; Boss, E. S. Climate-driven trends in contemporary ocean productivity. *Nature* **2006**, *444* (7120), 752–755.
- (12) Lommer, M.; Specht, M.; Roy, A.-S.; Kraemer, L.; Andresson, R.; Gutowska, M. A.; Wolf, J.; Bergner, S. V.; Schilhabel, M. B.; Klostermeier, U. C. Genome and low-iron response of an oceanic diatom adapted to chronic iron limitation. *Genome Biol.* **2012**, *13* (7), R66.
- (13) Allen, A. E.; LaRoche, J.; Maheswari, U.; Lommer, M.; Schauer, N.; Lopez, P. J.; Finazzi, G.; Fernie, A. R.; Bowler, C. Whole-cell response of the pennate diatom *Phaeodactylum tricornutum* to iron starvation. *Proc. Natl. Acad. Sci. U. S. A.* **2008**, *105* (30), 10438–10443.
- (14) Marchetti, A.; Schruth, D. M.; Durkin, C. A.; Parker, M. S.; Kodner, R. B.; Berthiaume, C. T.; Morales, R.; Allen, A. E.; Armbrust, E. V. Comparative metatranscriptomics identifies molecular bases for the physiological responses of phytoplankton to varying iron availability. *Proc. Natl. Acad. Sci. U. S. A.* **2012**, *109* (6), E317–E325.
- (15) Kustka, A. B.; Allen, A. E.; Morel, F. M. Sequence analysis and transcriptional regulation of Fe acquisition genes in two marine diatoms. *J. Phycol.* **2007**, *43* (4), 715–729.
- (16) Durkin, C. A.; Marchetti, A.; Bender, S. J.; Truong, T.; Morales, R.; Mock, T.; Armbrust, E. V. Frustule-related gene transcription and the influence of diatom community composition on silica precipitation in an iron-limited environment. *Limnol. Oceanogr.* **2012**, *57* (6), 1619–1633.
- (17) Mock, T.; Samanta, M. P.; Iverson, V.; Berthiaume, C.; Robison, M.; Holtermann, K.; Durkin, C.; BonDurant, S. S.; Richmond, K.; Rodesch, M. Whole-genome expression profiling of the marine diatom *Thalassiosira pseudonana* identifies genes involved in silicon bioprocesses. *Proc. Natl. Acad. Sci. U. S. A.* **2008**, *105* (5), 1579–1584.
- (18) Nunn, B. L.; Faux, J. F.; Hippmann, A. A.; Maldonado, M. T.; Harvey, H. R.; Goodlett, D. R.; Boyd, P. W.; Strzepek, R. F. Diatom proteomics reveals unique acclimation strategies to mitigate Fe limitation. *PLoS One* **2013**, *8* (10), e75653.
- (19) Thamatrakoln, K.; Korenovska, O.; Nihei, A. K.; Bidle, K. D. Whole-genome expression analysis reveals a role for death-related genes in stress acclimation of the diatom *Thalassiosira pseudonana*. *Environ. Microbiol.* **2012**, *14* (1), 67–81.
- (20) King, A. L.; Sanudo-Wilhelmy, S. A.; Boyd, P. W.; Twining, B. S.; Wilhelm, S. W.; Breene, C.; Ellwood, M. J.; Hutchins, D. A. A comparison of biogenic iron quotas during a diatom spring bloom using multiple approaches. *Biogeosciences* **2012**, *9*, 667–687.
- (21) Bidle, K. D.; Bender, S. J. Iron starvation and culture age activate metacaspases and programmed cell death in the marine diatom *Thalassiosira pseudonana*. *Eukaryot. Cell* **2008**, *7* (2), 223–236.
- (22) Whitney, L. P.; Lins, J. J.; Hughes, M. P.; Wells, M. L.; Chappell, P. D.; Jenkins, B. D. Characterization of putative iron responsive genes as species-specific indicators of iron stress in *Thalassiosiroid* diatoms. *Front. Microbiol.* **2011**, *2*, 1–14.
- (23) Leist, M.; Nicotera, P. The shape of cell death. *Biochem. Biophys. Res. Commun.* **1997**, *236* (1), 1–9.
- (24) Bidle, K. D.; Falkowski, P. G. Cell death in planktonic, photosynthetic microorganisms. *Nat. Rev. Microbiol.* **2004**, *2* (8), 643–655.
- (25) Vardi, A.; Berman-Frank, I.; Rozenberg, T.; Hadas, O.; Kaplan, A.; Levine, A. Programmed cell death of the dinoflagellate *Peridinium gatunense* is mediated by CO₂ limitation and oxidative stress. *Curr. Biol.* **1999**, *9* (18), 1061–1064.

- (26) Vardi, A.; Formiggini, F.; Casotti, R.; De Martino, A.; Ribalet, F.; Miralto, A.; Bowler, C. A stress surveillance system based on calcium and nitric oxide in marine diatoms. *PLoS Biol.* **2006**, *4* (3), 0411–0419.
- (27) Franklin, D. J.; Berges, J. A. Mortality in cultures of the dinoflagellate *Amphidinium carterae* during culture senescence and darkness. *Proc. R. Soc. London* **2004**, *271* (1553), 2099–2107.
- (28) Berges, J. A.; Falkowski, P. G. Physiological stress and cell death in marine phytoplankton: induction of proteases in response to nitrogen or light limitation. *Limnol. Oceanogr.* **1998**, *43* (1), 129–135.
- (29) Lane, N. Marine microbiology: origins of death. *Nature* **2008**, *453*, 583–585.
- (30) Brussaard, C. P.; Noordeloos, A. A.; Riegman, R. Autolysis kinetics of the marine diatom *Ditylum brightwellii* (Bacillariophyceae) under nitrogen and phosphorus limitation and starvation. *J. Phycol.* **1997**, *33* (6), 980–987.
- (31) Casotti, R.; Mazza, S.; Brunet, C.; Vantrepotte, V.; Ianora, A.; Miralto, A. Growth inhibition and toxicity of the diatom aldehyde 2-trans,4-trans-decadienal on *Thalassiosira weissflogii* (Bacillariophyceae). *J. Phycol.* **2005**, *41* (1), 7–20.
- (32) Chung, C.-C.; Hwang, S.-P. L.; Chang, J. Cooccurrence of ScDSP gene expression, cell death, and DNA fragmentation in a marine diatom, *Skeletonema costatum*. *Appl. Environ. Microbiol.* **2005**, *71* (12), 8744–8751.
- (33) Brussaard, C.; Riegman, R.; Noordeloos, A.; Cadée, G.; Witte, H.; Kop, A.; Nieuwland, G.; Van Duyl, F.; Bak, R. Effects of grazing, sedimentation and phytoplankton cell lysis on the structure of a coastal pelagic food web. *Mar. Ecol.: Prog. Ser.* **1995**, *123* (1), 259–271.
- (34) Cushing, D. H. The loss of diatoms in the spring bloom. *Philos. Trans. R. Soc. London, B* **1992**, *335* (1274), 237–246.
- (35) Apel, K.; Hirt, H. Reactive oxygen species: Metabolism, oxidative stress, and signal transduction. *Annu. Rev. Plant Biol.* **2004**, *55*, 373–399.
- (36) Mittler, R.; Vanderauwera, S.; Suzuki, N.; Miller, G.; Tognetti, V. B.; Vandepoel, K.; Gollery, M.; Shulaev, V.; Van Breusegem, F. ROS signaling: The new wave? *Trends Plant Sci.* **2011**, *16* (6), 300–309.
- (37) Korsmeyer, S. J.; Yin, X. M.; Yang, E.; Zha, J. P.; Oltvai, T. S. Z. BCL-2 gene family and the regulation of programmed cell death. *J. Cell. Biochem.* **1995**, *7*–7.
- (38) Levine, R. L.; Mosoni, L.; Berlett, B. S.; Stadtman, E. R. Methionine residues as endogenous antioxidants in proteins. *Proc. Natl. Acad. Sci. USA* **1996**, *93* (26), 15036–15040.
- (39) Vardi, A.; Bidle, K. D.; Kwityn, C.; Hirsh, D. J.; Thompson, S. M.; Callow, J. A.; Falkowski, P.; Bowler, C. A diatom gene regulating nitric-oxide signaling and susceptibility to diatom-derived aldehydes. *Curr. Biol.* **2008**, *18* (12), 895–899.
- (40) Mallick, N.; Mohn, F. H. Reactive oxygen species: Response of algal cells. *J. Plant Physiol.* **2000**, *157* (2), 183–193.
- (41) Ross, P. L.; Huang, Y. N.; Marchese, J. N.; Williamson, B.; Parker, K.; Hattan, S.; Khainovski, N.; Pillai, S.; Dey, S.; Daniels, S.; Purkayastha, S.; Juhasz, P.; Martin, S.; Bartlet-Jones, M.; He, F.; Jacobson, A.; Pappin, D. J. Multiplexed protein quantitation in *Saccharomyces cerevisiae* using amine-reactive isobaric tagging reagents. *Mol. Cell Proteomics* **2004**, *3*, 1154–1169.
- (42) Zieske, L. R. A perspective on the use of iTRAQ™ reagent technology for protein complex and profiling studies. *J. Exp. Bot.* **2006**, *57*, 1501–1508.
- (43) Liang, J.-R.; Ai, X.-X.; Gao, Y.-H.; Chen, C.-P. MALDI-TOF MS analysis of the extracellular polysaccharides released by the diatom *Thalassiosira pseudonana*. *J. Appl. Phycol.* **2013**, *25* (2), 477–484.
- (44) Du, C.; Liang, J.-R.; Chen, D.-D.; Xu, B.; Zhuo, W.-H.; Gao, Y.-H.; Chen, C.-P.; Bowler, C.; Zhang, W. iTRAQ-based proteomic analysis of the metabolism mechanism associated with silicon response in the marine diatom *Thalassiosira pseudonana*. *J. Proteome Res.* **2014**, *13*, 720–734.
- (45) Qiao, J.; Wang, J.; Chen, L.; Tian, X.; Huang, S.; Ren, X.; Zhang, W. Quantitative iTRAQ LC-MS/MS proteomics reveals metabolic responses to biofuel ethanol in cyanobacterial *Synechocystis* sp. PCC 6803. *J. Proteome Res.* **2012**, *11* (11), 5286–5300.
- (46) Van Domselaar, G. H.; Stothard, P.; Shrivastava, S.; Cruz, J. A.; Guo, A.; Dong, X.; Lu, P.; Szafron, D.; Greiner, R.; Wishart, D. S. BASys: a web server for automated bacterial genome annotation. *Nucleic Acids Res.* **2005**, *33* (suppl2), W455–W459.
- (47) Ye, J.; Coulouris, G.; Zaretskaya, I.; Cutcutache, I.; Rozen, S.; Madden, T. L. Primer-BLAST: a tool to design target-specific primers for polymerase chain reaction. *BMC Bioinform.* **2012**, *13*, 134.
- (48) Thornberry, N. A.; Lazebnik, Y. Caspases: Enemies within. *Science* **1998**, *281* (5381), 1312–1316.
- (49) Madeo, F.; Fröhlich, E.; Ligr, M.; Grey, M.; Sigrist, S. J.; Wolf, D. H.; Fröhlich, K.-U. Oxygen stress: a regulator of apoptosis in yeast. *J. Cell Biol.* **1999**, *145* (4), 757–767.
- (50) Lang, M.; Kroth, P. G. Diatom fucoxanthin chlorophyll a/c-binding protein (FCP) and land plant light-harvesting proteins use a similar pathway for thylakoid membrane insertion. *J. Biol. Chem.* **2001**, *276* (11), 7985–7991.
- (51) Zhu, S.-H.; Green, B. R. Photoprotection in the diatom *Thalassiosira pseudonana*: Role of LI818-like proteins in response to high light stress. *Biochim. Biophys. Acta* **2010**, *1797* (8), 1449–1457.
- (52) Bailleul, B.; Rogato, A.; De Martino, A.; Coesel, S.; Cardol, P.; Bowler, C.; Falciatore, A.; Finazzi, G. An atypical member of the light-harvesting complex stress-related protein family modulates diatom responses to light. *Proc. Natl. Acad. Sci. U. S. A.* **2010**, *107* (42), 18214–18219.
- (53) Treter, L.; Adam-Vizi, V. Alpha-ketoglutarate dehydrogenase: a target and generator of oxidative stress. *Philos. Trans. R. Soc. London, B* **2005**, *360* (1446), 2335–2345.
- (54) Sugioka, K.; Nakano, M.; Totsune-Nakano, H.; Minakami, H.; Tero-Kubota, S.; Ikegami, Y. Mechanism of O_2^- generation in reduction and oxidation cycle of ubiquinones in a model of mitochondrial electron transport systems. *Biochim. Biophys. Acta* **1988**, *936* (3), 377–385.
- (55) Turrens, J. F.; Boveris, A. Generation of superoxide anion by the NADH dehydrogenase of bovine heart mitochondria. *Biochem. J.* **1980**, *191*, 421–427.
- (56) Herrero, A.; Barja, G. Sites and mechanisms responsible for the low rate of free radical production of heart mitochondria in the long-lived pigeon. *Mech. Ageing Dev.* **1997**, *98* (2), 95–111.
- (57) St-Pierre, J.; Buckingham, J. A.; Roebuck, S. J.; Brand, M. D. Topology of superoxide production from different sites in the mitochondrial electron transport chain. *J. Biol. Chem.* **2002**, *277* (47), 44784–44790.
- (58) Varotsis, C.; Zhang, Y.; Appelman, E. H.; Babcock, G. T. Resolution of the reaction sequence during the reduction of O_2 by cytochrome oxidase. *Proc. Natl. Acad. Sci. U. S. A.* **1993**, *90* (1), 237–241.
- (59) Babcock, G. T.; Wikström, M. Oxygen activation and the conservation of energy in cell respiration. *Nature* **1992**, *356* (26), 301–309.
- (60) Chen, Q.; Vazquez, E. J.; Moghaddas, S.; Hoppel, C. L.; Lesnefsky, E. J. Production of reactive oxygen species by mitochondria central role of complex III. *J. Biol. Chem.* **2003**, *278* (38), 36027–36031.
- (61) Dawson, T. L.; Gores, G. J.; Nieminen, A.-L.; Herman, B.; Lemasters, J. J. Mitochondria as a source of reactive oxygen species during reductive stress in rat hepatocytes. *Am. J. Physiol.* **1993**, *264*, C961–C967.
- (62) Ken, C.-F.; Hsiung, T.-M.; Huang, Z.-X.; Juang, R.-H.; Lin, C.-T. Characterization of Fe/Mn-superoxide dismutase from diatom *Thalassiosira weissflogii*: cloning, expression, and property. *J. Agric. Food Chem.* **2005**, *53* (5), 1470–1474.
- (63) Chelikani, P.; Fita, I.; Loewen, P. Diversity of structures and properties among catalases. *Cell. Mol. Life Sci.* **2004**, *61* (2), 192–208.
- (64) Dietz, K.-J. Plant peroxiredoxins. *Annu. Rev. Plant Biol.* **2003**, *54* (1), 93–107.

- (65) Murata, H.; Ihara, Y.; Nakamura, H.; Yodoi, J.; Sumikawa, K.; Kondo, T. Glutaredoxin exerts an antiapoptotic effect by regulating the redox state of Akt. *J. Biol. Chem.* **2003**, *278* (50), 50226–50233.
- (66) Weber, T.; Gruber, A.; Kroth, P. G. The presence and localization of thioredoxins in diatoms, unicellular algae of secondary endosymbiotic origin. *Mol. Plant* **2009**, *2* (3), 468–477.
- (67) Itoh, H.; Komatsuda, A.; Ohtani, H.; Wakui, H.; Imai, H.; Sawada, K. i.; Otaka, M.; Ogura, M.; Suzuki, A.; Hamada, F. Mammalian HSP60 is quickly sorted into the mitochondria under conditions of dehydration. *Eur. J. Biochem.* **2002**, *269* (23), 5931–5938.
- (68) Kaufman, B. A.; Kolesar, J. E.; Perlman, P. S.; Butow, R. A. A function for the mitochondrial chaperonin Hsp60 in the structure and transmission of mitochondrial DNA nucleoids in *Saccharomyces cerevisiae*. *J. Cell Biol.* **2003**, *163* (3), 457–461.
- (69) Parker, M. S.; Armbrust, E. Synergistic effects of light, temperature, and nitrogen source on transcription of genes for carbon and nitrogen metabolism in the centric diatom *Thalassiosira pseudonana* (Bacillariophyceae). *J. Phycol.* **2005**, *41* (6), 1142–1153.
- (70) Miziorko, H. M.; Lorimer, G. H. Ribulose-1,5-bisphosphate carboxylase-oxygenase. *Annu. Rev. Biochem.* **1983**, *52* (1), 507–535.
- (71) Lundqvist, T.; Schneider, G. Crystal structure of activated ribulose-1,5-bisphosphate carboxylase complexed with its substrate, ribulose-1, 5-bisphosphate. *J. Biol. Chem.* **1991**, *266* (19), 12604–12611.
- (72) Van Lun, M.; Hub, J. S.; van der Spoel, D.; Andersson, I. CO₂ and O₂ distribution in rubisco suggests the small subunit functions as a CO₂ reservoir. *J. Am. Chem. Soc.* **2014**, *136* (8), 3165–3171.
- (73) Ameisen, J. C. On the origin, evolution, and nature of programmed cell death: a timeline of four billion years. *Cell Death Differ.* **2002**, *9* (4), 367–393.
- (74) Hedstrom, L. Serine protease mechanism and specificity. *Chem. Rev.* **2002**, *102* (12), 4501–4524.
- (75) Coffeen, W. C.; Wolpert, T. J. Purification and characterization of serine proteases that exhibit caspase-like activity and are associated with programmed cell death in *Avena sativa*. *Plant Cell Online* **2004**, *16* (4), 857–873.
- (76) Marzo, I.; Brenner, C.; Zamzami, N.; Jürgensmeier, J. M.; Susin, S. A.; Vieira, H. LA.; Prévost, M.-C.; Xie, Z. H.; Matsuyama, S.; Reed, J. C. Bax and adenine nucleotide translocator cooperate in the mitochondrial control of apoptosis. *Science* **1998**, *281* (5381), 2027–2031.
- (77) Bayles, K. W. Are the molecular strategies that control apoptosis conserved in bacteria? *Trends Microbiol.* **2003**, *11* (7), 306–311.
- (78) Lewis, K. Programmed death in bacteria. *Microbiol. Mol. Biol. Rev.* **2000**, *64* (3), 503–514.
- (79) Yarmolinsky, M. B. Programmed cell death in bacterial populations. *Science* **1995**, *267* (5199), 836–837.
- (80) Fröhlich, K.-U.; Madeo, F. Apoptosis in yeast—A monocellular organism exhibits altruistic behaviour. *FEBS Lett.* **2000**, *473* (1), 6–9.
- (81) Milligan, A. J.; Harrison, P. J. Effects of non-steady-state iron limitation on nitrogen assimilatory enzymes in the marine diatom *Thalassiosira weissflogii* (Bacillariophyceae). *J. Phycol.* **2000**, *36* (1), 78–86.
- (82) Allen, A. E.; Dupont, C. L.; Obornik, M.; Horak, A.; Nunes-Nesi, A.; McCrow, J. P.; Zheng, H.; Johnson, D. A.; Hu, H.; Fernie, A. R. Evolution and metabolic significance of the urea cycle in photosynthetic diatoms. *Nature* **2011**, *473* (7346), 203–207.
- (83) Rees, T.; Syrett, P. The uptake of urea by the diatom, *Phaeodactylum*. *New Phytol.* **1979**, *82* (1), 169–178.
- (84) Price, N. M.; Harrison, P. J. Uptake of urea C and urea N by the coastal marine diatom *Thalassiosira pseudonana*. *Limnol. Oceanogr.* **1988**, *33* (4), 528–537.